ISSN 1061-933X, Colloid Journal, 2013, Vol. 75, No. 3, pp. 253–260. © Pleiades Publishing, Ltd., 2013.
Original Russian Text © A.E. Galashev, 2013, published in Kolloidnyi Zhurnal, 2013, Vol. 75, No. 3, pp. 281–288.

IR and Raman Spectra of a Water–Methane Disperse System. Computer Experiment

A. E. Galashev

Institute of Industrial Ecology, Ural Branch, Russian Academy of Sciences, ul. Sof'i Kovalevskoi 20, Yekaterinburg, 620990 Russia

Received July 2, 2012

Abstract—Methane adsorption by water clusters is studied using a flexible molecule model. An increase in the number of methane molecules surrounding a water cluster leads to their structurization in its vicinity. The pattern of the frequency spectrum of complex permittivity strongly changes after methane molecules are captured by the disperse water system. The integral intensity of IR absorption grows with methane adsorption, whereas the Raman spectrum of the system is considerably depleted. Methane absorption markedly enhances the reflectivity and IR emission ability of the disperse system.

DOI: 10.1134/S1061933X1303006X

INTRODUCTION

Methane is of significant importance for various fields of science and technology, in particular, for geology, astrophysics, atmospheric physics, chemical kinetics and catalysis, chemical engineering, biotechnology, hydrogen production, environmental protection, etc. Methane is the basic component of natural gas and a very important greenhouse gas. The approximate contribution of methane to the changes in the radiation balance of the Earth's atmosphere is 0.48 W/m^2. The current methane content in the atmosphere is estimated to be ~1700 ppb that corresponds to the doubled preindustrial estimate [1]. Moreover, methane is an important component of the atmospheres of different planets including giant planets and satellites thereof. It is assumed that methane is a component of the Mars atmosphere [2]. Methane is in abundance on the planets discovered recently beyond the solar system and at brown dwarfs (the objects with masses intermediate between small-mass stars and giant planets) [3]. IR spectroscopy is the best diagnostic instrument for studying methane in the environment. Due to the high symmetry of a methane molecule, its complex electron structure consists of closely spaced levels [4]. The frequencies of four normal modes of methane are related approximately as follows: $\nu_1 \approx \nu_3 \approx 2\nu_2 \approx 2\nu_4$. As water is almost universal in the Solar System [5], the methane–water contacts change the spectroscopic characteristics of methane. The sum of the spectra of pure materials is known to differ from the spectrum of their mixture [6]. For example, the interaction of CH_4 with H_2O on the molecular level is accompanied by significant changes in the positions of peaks and spectral profiles in the near [6] and middle [7] IR regions. Therefore, in order to interpret the spectra of objects located outside the Solar System, we need to record spectra of CH_4 and H_2O upon their intermolecular interaction.

Methane–water systems play important roles in the practical application of organic fuel (in the form of clathrates), conversion of solar energy (thermochemistry), or methane formation in fermentation reactions [8]. Under environmental conditions, the free energy of hydration of small nonpolar molecules, such as methane, is mainly determined by the entropy component and depends, to a greater extent, on the number of the types of arrangement of all water molecules in a hydrate layer of methane rather than on their energy [9]. In the vicinity of small nonpolar molecules, water molecules can rearrange themselves to encapsulate a quest molecule and reform ruptured H bonds [10, 11].

To date, the main attention has been focused on studying the properties of extended liquid solutions and hydrates of methane (water ices containing large amounts of methane) and few works have dealt with the cluster hydrophobic effect in the atmosphere [12–14]. Small water clusters composed of 10 and 20 molecules have been considered in those studies. Water molecules have been shown to be immiscible with adsorbed methane molecules.

The aim of this work was to study the changes that take place in IR and Raman spectra upon methane adsorption on water clusters.

MOLECULAR DYNAMICS MODEL

The interaction of water molecules in clusters was described by a nonadditive potential, the additive component of which was represented by the modified in [15] TIP4P potential for water [16], while the nonadditive component was determined by the polarization interaction. Based on the data of [15], we assumed

that, for water molecule, the permanent dipole moment is equal to its experimental value of 1.848 D. The geometry of H_2O molecule corresponds to the following experimental molecular parameters in a gas phase: the distance between hydrogen and oxygen atoms is $r_{OH} = 0.09572$ nm and H–O–H angle is 104.5° [17]. Fixed charges ($q_H = 0.519e$, $q_M = -1.038e$) are assigned to H atoms and point M_0 located at the bisector of the H–O–H angle at a distance of 0.0215 nm from the oxygen atom. The charges and the position of point M_0 were chosen so as to reproduce the experimental values of the dipole and quadrupole moments [18, 19], as well as the calculated ab initio energy of a dimer and characteristic distances in it [20]. Stabilization of the short-range order in water clusters is, to a great extent, attained due to the short-range Lennard-Jones potential, with the interaction center being attributed to the oxygen atom. Along with the electric charge, the polarizability, which is needed for the description of the nonadditive polarization energy, was related to point M_0. Induced dipole moments $\mathbf{d}_i$ were calculated using the standard iteration procedure at each time step [15]. The accuracy of $\mathbf{d}_i$ determination was preset in the range of 10^{-5}–10^{-4} D.

The methane–methane interatomic interactions were determined by the Lennard-Jones and Coulomb contributions as follows:

$$\Phi_{ij}(r) = \varepsilon_{ij}\left[\left(\frac{r_0}{r_{ij}}\right)^{12} - 2\left(\frac{r_0}{r_{ij}}\right)^{6}\right] + \frac{q_i q_j}{r_{ij}}.$$

Parameters ε_{ij}, r_0, and q_i for H and C atoms in the CH_4 molecule were taken equal to 0.038 kcal/mol, 0.28525 nm, and $0.119e$ and 0.07382 kcal/mol, 0.43 nm, and $-0.476e$, respectively [21]. The parameters of the Lennard-Jones potential describing methane–water interactions were determined by the Berthelot–Lorentz formulas

$$\varepsilon_{aw}^{(LJ)} = \sqrt{\varepsilon_a^{(LJ)}\varepsilon_w^{(LJ)}}, \quad \sigma_{aw}^{(LJ)} = \frac{\sigma_a^{(LJ)} + \sigma_w^{(LJ)}}{2},$$

where $\varepsilon_a^{(LJ)}$, $\varepsilon_w^{(LJ)}$ are energy parameters and $\sigma_a^{(LJ)}$, $\sigma_w^{(LJ)}$ are the geometric parameters of the potential for C and H atoms in methane molecule and O atom in water molecule, respectively.

Methane molecule has the shape of a tetrahedron with carbon atom located in the center and hydrogen atoms in the vertexes. The H–C–H bond angle is equal to the tetrahedral angle of 109°. The interatomic distances in the CH_4 molecule were $r_{CH} = 0.109$ nm and $r_{HH} = 0.177$ nm. The nonpolar CH_4 molecule has a higher polarizability α^p (2.6 Å^3) than does the water molecule (1.49 Å^3) [22].

The trajectories of the mass centers of the molecules were determined by the fourth-order Gear method [23]. Time step Δt of integration was 0.2×10^{-16} s. In a molecular-dynamics calculation $2 \times 10^6\,\Delta t$ long, the equilibration was preliminarily performed at $T =$ 233 K for pure water clusters free of impurity molecules. The $(H_2O)_{50}$, cluster configuration at the 40-ps time moment was further used as the initial configuration for simulating $(CH_4)_i(H_2O)_{50}$ heteroclusters with $1 \le i \le 6$. Each added CH_4 molecule was initially placed into a position such that the shortest distance between the atoms of this molecule and atoms of water molecules was nearly 0.6 nm. At the beginning, the mass centers of CH_4 molecules were placed in coordinate axes outside the water cluster. The initial orientation of methane molecules was arbitrary. A newly formed cluster was equilibrated within a time interval of $1.2 \times 10^6\,\Delta t$ at $T = 233$ K; after that, the desired physicochemical properties were calculated at the same temperature within an interval of $2.5 \times 10^6\,\Delta t$. A system of $(CH_4)_i(H_2O)_{50}$ clusters was formed in accordance with cluster statistical weights, which were determined as follows. Let us consider the case of unpolarized light scattering, when free path l of molecules is much shorter than light wavelength λ. Extinction (attenuation) ratio h of an incident beam is determined by, on the one hand, the Rayleigh formula [24], and, on the other hand, scattering coefficient ρ ($h = \frac{16\pi}{3}\rho$) [25] under an approximation of the scattering angle of 90°. Taking into account that $h = \alpha + \rho$, where α is the absorption coefficient, we have

$$N = \frac{2\omega^4}{3\pi c^4}\frac{\left(\sqrt{\varepsilon}-1\right)^2}{\alpha}\left(1 - \frac{3}{16\pi}\right),$$

where N is the number of scattering centers per cubic centimeter. Here c is the speed of light, ε is medium dielectric permittivity, and ω is the frequency of the incident wave.

Let us define the following types of ultradisperse systems: system I is a monodisperse system of $(H_2O)_{50}$; clusters, system II is a region filled with water clusters having sizes of 10–50 molecules (the number of molecules in a cluster is increased with step $\Delta n = 5$), and system III is a medium composed of $(H_2O)_{50}$ clusters that contain from one to six adsorbed CH_4 molecules.

We form these systems in a manner such that a cluster containing i impurity molecules and n water molecules has the following statistical weight:

$$W_{in} = \frac{N_{in}}{N_{l\Sigma}}, \quad 1 \le i \le 6, \quad 10 \le n \le 50 \quad (\Delta n = 5),$$

where N_{in} is the number of clusters containing n water molecules and i CH_4 molecules in 1 cm^3 and l acquires values of 1 and 2: $N_{1\Sigma} = \sum_{n=1}^{9} N_{i=0,n}$, $N_{2\Sigma} = \sum_{i=1}^{6} N_{i,n=50}$. Thereafter, all spectral characteristics are calculated with regard to accepted statistical weights W_{in}.

The motion equations for molecular rotation are analytically solved using the Rodrigo–Hamilton parameters [26], and the integration of equations of motion involving rotations is implemented according to the Sonnenschein approach [27].

DIELECTRIC PROPERTIES

Static dielectric permittivity ε_0 was calculated via fluctuations of total dipole moment $\mathbf{M}$ [28] as follows:

$$\varepsilon_0 = 1 + \frac{4\pi}{3VkT}\left[\left\langle \mathbf{M}^2 \right\rangle - \left\langle \mathbf{M} \right\rangle^2\right],$$

where V is the cluster volume and k is Boltzmann's constant.

Dielectric permittivity $\varepsilon(\omega)$ as a function of frequency ω was represented by complex value $\varepsilon(\omega) = \varepsilon'(\omega) - i\varepsilon''(\omega)$, which was determined by the following equation [28, 29]:

$$\frac{\varepsilon(\omega) - 1}{\varepsilon_0 - 1} = -\int_0^\infty \exp(-i\omega t)\frac{dF}{dt}dt$$
$$= 1 - i\omega\int_0^\infty \exp(-i\omega t)C(t)dt,$$

where the $C(t)$ function is the normalized autocorrelation function of the total cluster dipole moment,

$$C(t) = \frac{\left\langle \mathbf{M}(t)\cdot\mathbf{M}(0)\right\rangle}{\left\langle \mathbf{M}^2\right\rangle}.$$

Coefficient α of absorption of external IR radiation can be expressed via the imaginary component of frequency-dependent dielectric permittivity $\varepsilon(\omega)$ in the following form [30]:

$$\alpha(\omega) = 2\frac{\omega}{c}\mathrm{Im}\left[\varepsilon(\omega)^{1/2}\right].$$

In the case of depolarized light, the Raman spectrum $J(\omega)$ is specified by the following expression [31] (the scatterings at $\omega < 0$ and $\omega > 0$ are of the Stokes and anti-Stokes types, respectively):

$$J(\omega) = \frac{\omega}{(\omega_L - \omega)^4}\left(1 - e^{-\hbar\omega/kT}\right)$$
$$\times\ \mathrm{Re}\int_0^\infty dt e^{i\omega t}\left\langle \Pi_{xz}(t)\Pi_{xz}(0)\right\rangle,$$

where

$$\Pi(t) \equiv \sum_{j=1}^{N}\left[\boldsymbol{\alpha}_j(t) - \left\langle \boldsymbol{\alpha}_j\right\rangle\right],$$

ω_L is the exciting laser frequency, Π_{xz} is the xz component of the $\Pi(t)$ value, the x axis is directed along the molecular dipole, and xOy is the molecular plane. The value ω_L = 19 436.3 cm^{-1} (green line of argon laser, λ = 514.5 nm) was used in the simulation.

Reflection coefficient R is determined as the ratio between the average energy flux reflected from a surface and the incident flux. At the normal incidence of a plane monochromatic wave, the reflection coefficient is determined by the following formula [24]:

$$R = \left|\frac{\sqrt{|\varepsilon_1|} - \sqrt{|\varepsilon_2|}}{\sqrt{|\varepsilon_1|} + \sqrt{|\varepsilon_2|}}\right|^2. \quad (1)$$

Here, it is assumed that the wave incidence occurs from a transparent medium (medium 1) into a medium that may be both transparent and nontransparent, i.e., an absorbing and scattering one (medium 2). The subscripts at the dielectric permittivity in Eq. (1) denote corresponding media.

The frequency dispersion of the dielectric permittivity determines the frequency dependence of dielectric loss $P(\omega)$ according to the following expression [25]:

$$P = \frac{\varepsilon''\left\langle E^2\right\rangle\omega}{4\pi},$$

where $\langle E^2\rangle$ is the mean-square electric field strength and ω is the frequency of the emitted electromagnetic wave.

The motions at a frequency below 1200 cm^{-1} correspond to molecular librations, while frequencies above 1200 cm^{-1} describe mainly intramolecular vibrations [32] realized in the following approximation. Flexible molecular models were considered. Molecules were provided with flexibility via the procedure developed in [33–35] within the framework of the Hamilton dynamics: the deformation of a molecule was determined by equilibrating total potential force $\mathbf{f}(\mathbf{u}) = -\frac{\partial\mathbf{r}}{\partial\mathbf{u}}\nabla\Phi(\mathbf{r})$ with centrifugal force $-\ -\mu u\omega^2$, where μ is the reduced mass, u is the distance between two atoms, ω is the vibration frequency, and $\mathbf{r}$ determines the point at which the force is applied.

SIMULATION RESULTS

As a result of adsorption of i methane molecules by a water cluster, a $(CH_4)_i(H_2O)_{50}$. cluster is formed. The configuration of a $(CH_4)_6(H_2O)_{50}$, cluster containing six CH_4 molecules at the 50-ps time moment is exemplified in Fig. 1. Methane molecules are arranged symmetrically relative to the cluster center in the vertical and horizontal directions. They have rather arbitrary orientations that are determined by the position and orientation of neighboring water molecules. As the tetrahedral CH_4 molecule carries external positive electric charges (on H atoms), the tetrahedron vertex is located closer to the negatively charged oxygen atom of a nearest water molecule. The situations, in which H atoms of methane molecule are located near O at-

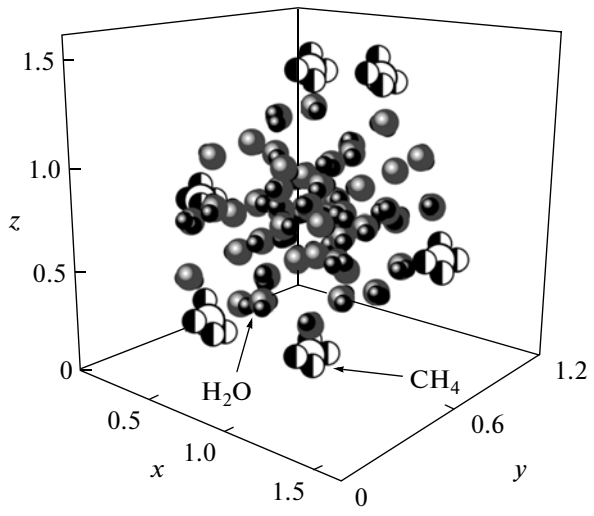

Fig. 1. Configuration of $(CH_4)_6(H_2O)_{50}$, cluster at the 50-ps time moment.

oms of two or even three H_2O molecules, are also possible. The symmetrical arrangement of hydrophobic methane molecules results in the densification of the water component of the cluster, which affects its optical properties.

The frequency spectra of the real and imaginary components of the dielectric permittivity are considerably transformed after adsorption of CH_4 molecules by water clusters (Fig. 2). While, for a system composed of identical water clusters $(H_2O)_{50}$ (system I) or a system of water clusters with different sizes $(H_2O)_{n=10,\ldots,50}$ (system II), the $\varepsilon'(\omega)$ and $\varepsilon''(\omega)$ functions rapidly increase in the beginning of the frequency range (below 1100 cm^{-1}), for the system of water clusters containing methane molecules $(CH_4)_{i=1,\ldots,6}(H_2O)_{50}$ (system III), these functions grow nonmonotonically to maximum values in the vicinity of 3280 and 3070 cm^{-1}, respectively, with the most pronounced increase in $\varepsilon'(\omega)$ and $\varepsilon''(\omega)$ values beginning from frequencies of 2875 and 2500 cm^{-1}, respectively. The maximum values of $\varepsilon'(\omega)$ and $\varepsilon''(\omega)$ for system III exceed the analogous characteristics for systems I and II. The $\varepsilon'(\omega)$ function calculated in [30] for bulk liquid water decreases monotonically in the frequency range of $200 \le \omega \le 3500$ cm^{-1}, whereas the experimental $\varepsilon''(\omega)$ function [36] exhibits a nonmonotonic decrease down to ≈930 cm^{-1}, followed by a monotonic decay.

Figure 3 shows the frequency dependences of absorption coefficient α for systems I–III. The integral intensities of the $\alpha(\omega)$ spectra for these systems are related as 1 : 0.80 : 1.04. The main maxima of the spectra fall in the frequency range of 3270–3500 cm^{-1}. The $\alpha(\omega)$ spectra of liquid water [37] and an $H_2O/CH_4 = 20$ solid mixture at $T = 15$ K [6] lie in the same range. The IR absorption spectra of CH_4 and

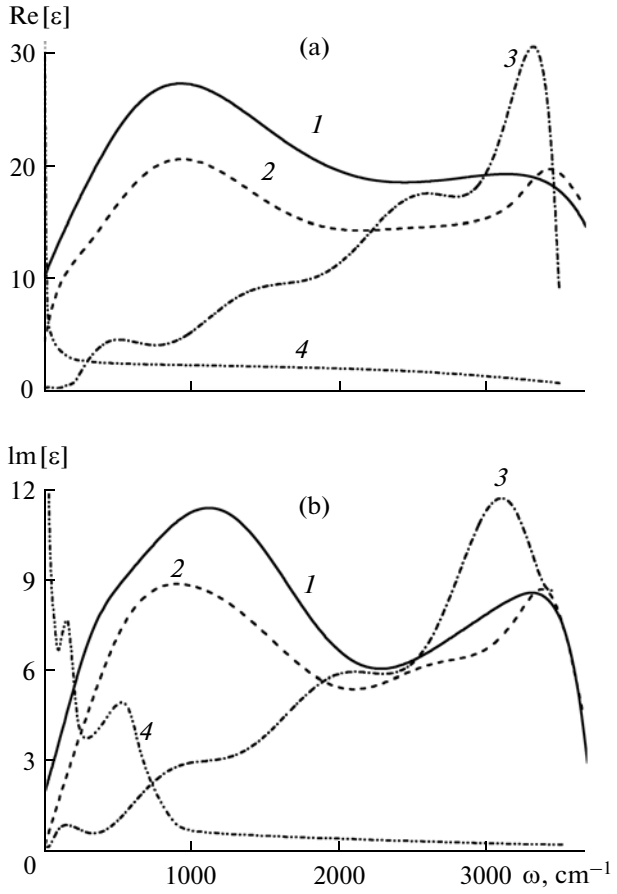

Fig. 2. The (a) real and (b) imaginary components of dielectric permittivity for different cluster systems: (*1*) I, (*2*) II, and (*3*) III. Curves (*4*) refer to the components of dielectric permittivity of liquid water obtained (a) by molecular dynamics calculations [30] and (b) in experiments [36].

CD_4 captured in the matrix of an inert gas at low temperatures exhibit maxima in the regions of 3015 and 994 cm^{-1}, respectively [38]. The frequency range of $2750 \le \omega \le 3300$ cm^{-1} is of particular importance, because it contains characteristic frequencies of stretching vibrations for molecules comprising carbon–hydrogen bonds. In the homologous series of hydrocarbons, the methane molecule is unique, because all C–H bonds belong to the same group, in contrast to, e.g., hexane, which comprises bonds of several types.

Figure 4 shows $\alpha(\omega)$ spectra for individual clusters. As a rule, the addition of CH_4 molecules to a $(H_2O)_{50}$ cluster leads to a decrease in the integral intensity I_α of the $\alpha(\omega)$ spectrum. The I_α values for $(CH_4)_i(H_2O)_{50}$ clusters with $i = 0$–6 are related as 1 : 1.06 : 0.95 : 0.44 : 0.94 : 0.96 : 1.17. It is seen that, when one or six CH_4 molecules are added to a water cluster, I_α increases. The addition of CH_4 molecules is accompanied by a

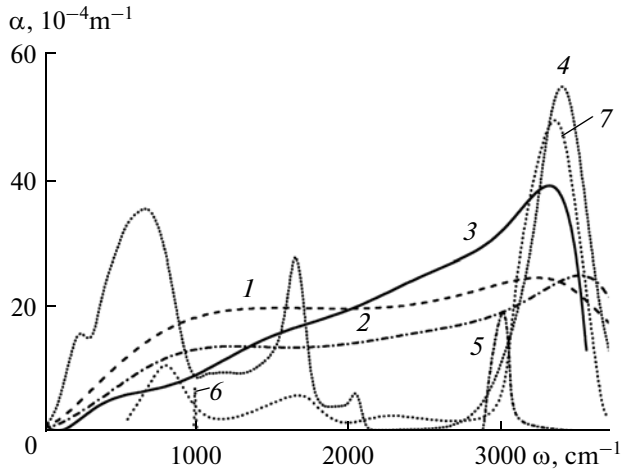

Fig. 3. IR absorption coefficients α(ω) for systems (*1*) I, (*2*) II, and (*3*) III; (*4*) absorption coefficient experimentally determined for bulk liquid water [37]; absorption spectra of (*5*) CH_4 and (*6*) CD_4 captured in an inert gas matrix [38]; and (*7*) α(ω) spectrum of solid mixture $[H_2O]/[CH_4] = 20$ at $T = 15$ K [6].

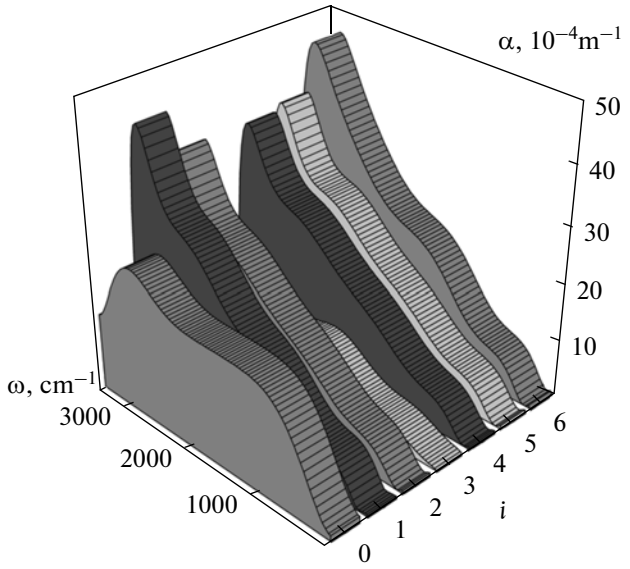

Fig. 4. IR absorption coefficients for $iCH_4 + (H_2O)_{50}$, cluster subsystems, $0 \le i \le 6$.

blue shift of the main peak in the α(ω) spectrum, with the shift being the same in all cases except for $i = 3$.

Figure 5 exhibits Raman spectra $J(\omega)$ calculated for systems I and III and the experimental spectrum of liquid water measured at 300 K [39]. The adsorption of CH_4 molecules by $(H_2O)_{50}$ clusters leads to a significant reduction in the number and intensity of the peaks. The comparison of the $J(\omega)$ spectra for systems I and III shows that only a peak at 3117 cm^{-1} is well reproducible (with a weak blue shift). This peak exhibits a red shift (by ≈200 cm^{-1}) relative to the main peak in the $J(\omega)$ spectrum of liquid water. In the case of pure water, different arrangements of oxygen atoms with tetrahedral coordination and variability of hydrogen bond lengths and angles result in the formation of various ice phases. The incorporation of different guest molecules into the structural cavities of the polyhedral skeleton of water yields more than ten stable structures, which are divided into gas hydrates of three types denoted as sI, sII and sH structures [40]. Pure methane hydrate forms, as a rule, a cubic sI structure, in which small methane molecules are easily accommodated in both large and small cavities. At pressures and temperatures higher than those for the sI structure, two other forms, sII and sH, are stable [41]. As a result of compression, methane hydrate sI is transformed into the sII phase at 100 MPa and, then, into the sH phase at 600 MPa. The Raman spectra of these different forms of methane hydrate are quite different (see inset in Fig. 5). The main peaks of the three forms of methane hydrate show a red shift on the order of 200–213 cm^{-1} relative to the main peak in the $J(\omega)$ spectrum of system III.

The reflection of IR radiation by disperse systems I–III is characterized by the $R(\omega)$ spectra (Fig. 6). System II, which consists of water clusters with different sizes, has average reflection coefficient $\bar{R} = 0.35$ and frequency of most strongly reflected photons $\omega_R = 1015$ cm^{-1}. For system I, $\bar{R} = 0.41$ and $\omega_R = 976$ cm^{-1}, while, for system III, $\bar{R} = 0.74$ and $\omega_R = 3255$ cm^{-1}. Thus, the adsorption of CH_4 molecules by the system of $(H_2O)_{50}$ clusters causes a 1.8-fold increase in reflection coefficient $\bar{R}$ and a considerable blue shift of the frequency of the most efficiently reflected radiation.

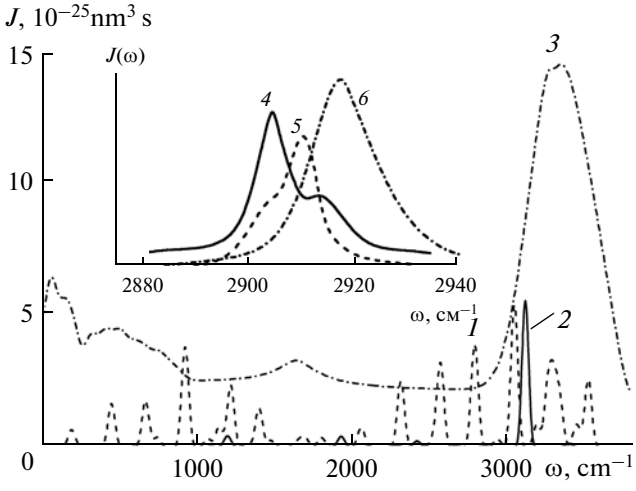

Fig. 5. Experimental Raman spectra for systems (*1*) I and (*2*) III and (*3*) liquid water at 293 K [39] and (*4–6*) experimental spectra of sI, sII and sH methane hydrates, respectively [40].

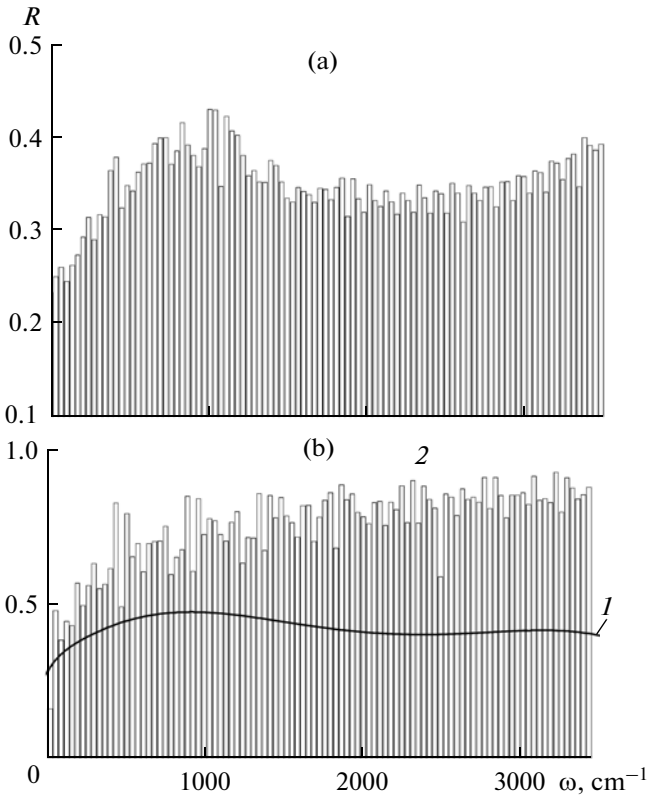

Fig. 6. Coefficients of monochromatic plane electromagnetic-wave reflection by different disperse systems: (a) II and (b) (*1*) I and (*2*) III.

Figure 7 shows IR emission spectra $P(\omega)$ for systems I–III along with the laboratory emission spectrum of methane at 800 K [42]. The integral intensity ratio between the $P(\omega)$ spectra for systems I–III is 1 : 0.77 : 1.68, and the main peaks are positioned at 3340, 3471, and 3099 cm^{-1}. Thus, the addition of CH_4 molecules to $(H_2O)_{50}$ clusters is accompanied by a red shift of the main peak by 241 cm^{-1}. The position of the main peak for system III is in good accordance with that of the main peak of the experimental emission spectrum of methane (3087 cm^{-1}). Note that weak bands to the left and right of the $P(\omega)$ spectrum of methane (Fig. 7) were ignored in [42].

Intensities I_P of emission spectra of individual $(CH_4)_i(H_2O)_{50}$ clusters are widely varied (Fig. 8). For example, as i increases from 0 to 6, the I_P values appear to be related as 1 : 0.53 : 0.57 : 0.21 : 1.21 : 1.39 : 1.76; i.e., the maximum I_P value (at $i = 6$) is larger than the minimum one (at $i = 3$) by a factor of 8.2. At the same time, the pattern of the $P(\omega)$ spectrum dramatically changes only upon the addition of the first CH_4 molecule to an $(H_2O)_{50}$ cluster.

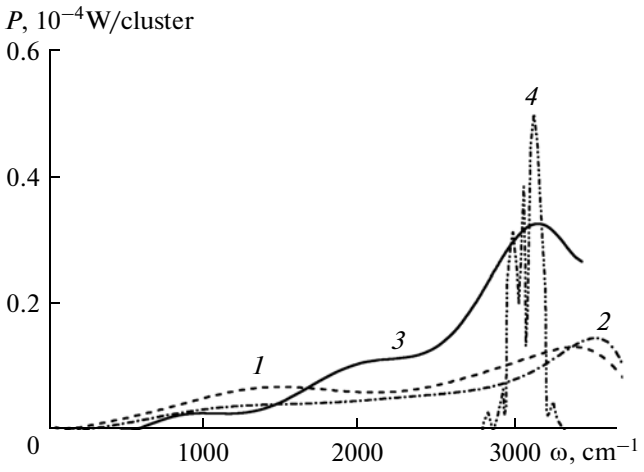

Fig. 7. IR emission spectra for systems (*1*) I, (*2*) II, and (*3*) III and (*4*) emission spectrum of methane measured in laboratory experiments at 800 K [42].

DISCUSSION

The addition of methane to water clusters leads to an essential change in the $\alpha(\omega)$ spectrum such that the position of the main spectral peak is shifted to the corresponding peak of the $\alpha(\omega)$ spectrum for the mechanical CH_4–H_2O mixture, in which molecular mixing is absent. This approach of the spectra is likely related to the fact that simple CH_4 hydrocarbon does not form hydrogen bonds with H_2O. The disperse aqueous medium containing absorbed methane is distinguished by a high background intensity of the $\alpha(\omega)$ spectrum. Therefore, the form of each component of a CH_4–H_2O mixture should be judged based on the combination of characteristic spectral features rather than from peak positions alone. In the absence of molecular mixing in the CH_4–H_2O mechanical mixture, thermal effects related to a great difference (≈182 K) between the melting temperatures of these components can be observed at low temperatures. The presence of CH_4 molecules in water clusters is distinguished by a considerable decrease in intensity of the Raman spectral bands down to the disappearance of many of them in the range of $\omega < 3000$ cm^{-1}. The spectrum displays only one distinct band remaining from the spectrum of water clusters, which exhibits a blue shift by 200–213 cm^{-1}relative to the corresponding band in the Raman spectra of different forms of methane hydrate.

The data obtained in this work may be used for verification of the ab initio quantum chemical calculations and analysis of spectra in astrophysics, for example, when studying brown dwarfs and hot planets outside the Solar System. The near IR spectra of *T*-class brown dwarfs display a lot of bands due to methane and water [43]. The bands of methane are identified by comparing with the spectrum of Jupiter or a spectrum obtained by numerical simulation. It is common

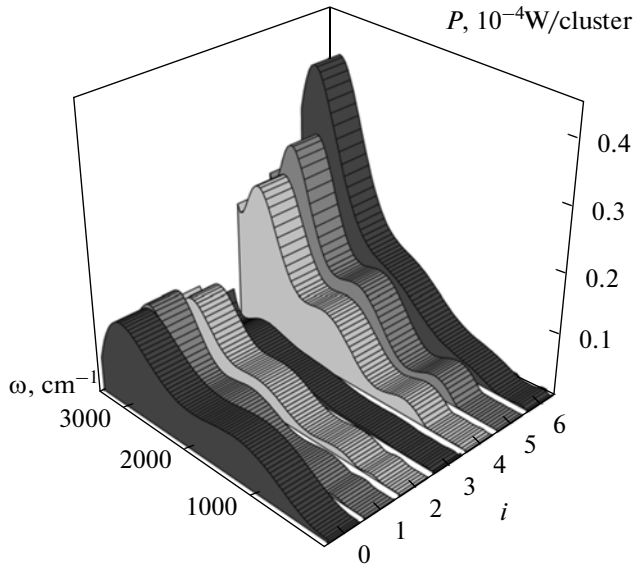

Fig. 8. IR emission spectra for $(CH_4)_i(H_2O)_{50}$, clusters, $0 \le i \le 6$.

knowledge that the equilibrium concentrations in the $CO + 3H_2 \leftrightarrow CH_4 + H_2O$ reaction are strongly temperature-dependent; therefore, the ν_3 band can be an efficient indicator of temperature [44]. The relation between the populations of methane and CO at a given pressure can also be an indicator of the temperature of brown dwarfs [45]. The availability of laboratory and model spectra of methane–water mixtures can help to determine the atmosphere composition of brown dwarfs and their temperature and gravitational forces [46].

CONCLUSIONS

Methane adsorption by disperse aqueous medium has been studied in terms of a molecular-dynamics model of flexible molecules. An increase in the molar fraction of methane near a $(H_2O)_{50}$ cluster leads, in the long run, to the structurization of CH_4 molecules in the vicinity of the cluster. The integral absorption coefficient $\alpha(\omega)$ in the IR region increases with methane adsorption by the disperse aqueous medium. Therewith, the main absorption band shifts toward the position of the most intense band in the IR spectrum of gaseous methane. On the contrary, the number and intensity of bands dramatically decrease in the Raman spectrum of the disperse methane-containing system. In fact, only one meaningful band remains preserved in the $J(\omega)$ spectrum. As spherically symmetrical CH_4 molecules are adsorbed by the disperse aqueous system, its reflectivity noticeably increases and the frequency distribution of reflection coefficient becomes more uniform. The emission intensity of the water–methane disperse system markedly increases, especially in the high-frequency region of the $P(\omega)$ spectrum. The position of the main maximum in the $P(\omega)$ spectrum of this system is in good agreement with the position of the maximum in the emission spectrum of methane measured under laboratory conditions. Because of different selection rules, the calculated $\alpha(\omega)$ and $J(\omega)$ spectra may appear to be useful for the solution of some problems, including astrophysical ones.

REFERENCES

1. Khalin, M.A. and Rasmussen, R.A., *Atmos. Environ.*, 1987, vol. 21, p. 2445.
2. Formisano, V., Atreya, S., Encrenaz, T., Ignatiev, N., and Giuranna, M., *Science* (Washington, D. C.), 2004, vol. 306, p. 1758.
3. Swain, M.R., Vasisht, G., and Tinetti, G., *Nature* (London), 2008, vol. 452, p. 329.
4. Boudon, V., Rey, M., and Loete, M., *J. Quant. Spectrosc. Radiat. Transfer*, 2006, vol. 98, p. 394.
5. Roush, T.L., *J. Geophys. Res.*, 2001, vol. 106, p. 33315.
6. Bernstein, M.P., Cruikshank, D.P., and Sandford, S.A., *Icarus*, 2006, vol. 181, p. 302.
7. Hudgins, D.M., Sandford, S.A., Allamandola, L.J., and Tielens, A.G.G.M., *Astrophys. J., Suppl. Ser.*, 1993, vol. 86, p. 713.
8. Laaksonen, A. and Stilbs, P., *Mol. Phys.*, 1991, vol. 74, p. 747.
9. Chandler, D., *Nature* (London), 2002, vol. 417, p. 491.
10. Chau, P.L. and Mancera, R.L., *Mol. Phys.*, 1999, vol. 96, p. 109.
11. Lambeth, B.P., Jr., Junghans, C., Kremer, K., Clementi, C., and Delle Site, L., *J. Chem. Phys.*, 2010, vol. 133, p. 221101.
12. Galashev, A.Y., *Mol. Simul.*, 2010, vol. 36, p. 273.
13. Galashev, A.E., Chukanov, V.N., Novruzov, A.N., and Novruzova, O.A., *Teplofiz. Vys. Temp.*, 2006, vol. 44, p. 370.
14. Galashev, A.E., Novruzov, A.N., and Galasheva, A.A., *Khim. Fiz.*, 2006, vol. 25, p. 26.
15. Dang, L.X. and Chang, T.-M., *J. Chem. Phys.*, 1997, vol. 106, p. 8149.
16. Jorgensen, W.L. and Madura, J.D., *J. Am. Chem. Soc.*, 1983, vol. 105, p. 1407.
17. Benedict, W.S., Gailar, N., and Plyler, E.K., *J. Chem. Phys.*, 1956, vol. 24, p. 1139.
18. Xantheas, S., *J. Chem. Phys.*, 1996, vol. 104, p. 8821.
19. Feller, D. and Dixon, D.A., *J. Chem. Phys.*, 1996, vol. 100, p. 2993.
20. Smith, D.E. and Dang, L.X., *J. Chem. Phys.*, 1994, vol. 100, p. 3757.
21. New, M.H. and Berne, B.J., *J. Am. Chem. Soc.*, 1995, vol. 117, p. 7172.
22. *Spravochnik khimika. T. 1* (Chemist's Handbook), Nikol'skii, B.P., Ed., Leningrad: Khimiya, 1971, vol. 1.
23. Haile, J.M., *Molecular Dynamics Simulation. Elementary Methods*, New York: Wiley, 1992.
24. Landau, L., Lifshitz, E., and Pitaevski, L., *Electrodyinamics of Continuous Media*, Oxford: Pergamon, 1984.
25. *Fizicheskaya entsiklopediya. T. 1* (Physical Encyclopedia), Prokhorov, A.M., Ed., Moscow: Sovetskaya Entsiklopediya, 1988, vol. 1.

26. Koshlyakov, V.N., *Zadachi dinamiki tverdogo tela i prikladnoi teorii giroskopov* (Problems of Solid Body Dynamics and Applied Theory of Gyroscopes), Moscow: Nauka, 1985.
27. Sonnenschein, R., *J. Comput. Phys.*, 1985, vol. 59, p. 347.
28. Bresme, F., *J. Chem. Phys.*, 2001, vol. 115, p. 7564.
29. Neumann, M., *J. Chem. Phys.*, 1985, vol. 82, p. 5663.
30. Neumann, M., *J. Chem. Phys.*, 1986, vol. 85, p. 1567.
31. Bosma, W.B., Fried, L.E., and Mukamel, S., *J. Chem. Phys.*, 1993, vol. 98, p. 4413.
32. Stern, H.A. and Berne, B.J., *J. Chem. Phys.*, 2001, vol. 115, p. 7622.
33. Lemberg, H.L. and Stillinger, F.H., *J. Chem. Phys.*, 1975, vol. 62, p. 1677.
34. Rahman, A., Stillinger, F.H., and Lemberg, H.L., *J. Chem. Phys.*, 1975, vol. 63, p. 5223.
35. Saint-Martin, H., Hess, B., and Berendsen, H.J.C., *J. Chem. Phys.*, 2004, vol. 120, p. 11133.
36. Angell, C.A. and Rodgers, V., *J. Chem. Phys.*, 1984, vol. 80, p. 6245.
37. Goggin, P.L. and Carr, C., in *Water and Aqueous Solutions*, Neilson, G.W. and Enderby, J.E, Eds., Bristol: Adam Hilger, 1986, vol. 37, p. 149.
38. Chamberland, A., Belzile, R., and Cabana, A., *Can. J. Chem.*, 1970, vol. 48, p. 1129.
39. Vallee, P., Lafait, J., Ghomi, M., Jouanne, M., and Morhange, J.F., *J. Mol. Struct.*, 2003, vols. 651–653, p. 371.
40. Chou, I.-M., Sharma, A., Burruss, C., Shu, J., Mao, H.-K., Hemley, R.J., Goncharov, F., Stern, L.A., and Kirby, H., *Proc. Natl. Acad. Sci. U. S. A.*, 2000, vol. 97, p. 13484.
41. Ripmeester, J.A., Ratcliffe, C.I., Klug, D.D., and Tse, J.S., *Ann. N. Y. Acad. Sci.*, 1994, vol. 715, p. 161.
42. Nassar, R. and Bernath, P., *J. Quant. Spectrosc. Radiat. Transfer*, 2003, vol. 82, p. 279.
43. Goodwin, S.P. and Whitworth, A., *Astron. Astrophys.*, 2007, vol. 466, p. 943.
44. Geballe, T.R., Noll, K.S., Leggett, S.K., Knapp, G.R., Fan, X., and Golimowski, D., in *Ultracool Dwarfs: New Spectral Types L and T*, Jones, H.R.A. and Steele, I.A, Eds., Berlin: Springer, 2001, p. 83.
45. Lodders, K. and Fegley, B., Jr., *Icarus*, 2002, vol. 155, p. 393.
46. Sengupta, S. and Krishan, V., *Astron. Astrophys.*, 2000, vol. 358, p. L33.

Translated by L. Tkachenko